Electronic Supplementary Information

Probing Halogen Bonds with Solid-State NMR Spectroscopy. Observation and Interpretation of $J(^{77}Se, ^{31}P)$ Coupling in Halogen-Bonded P=Se···I Motifs

Jasmine Viger-Gravel, Julia E. Meyer, Ilia Korobkov, and David L. Bryce*

*Author to whom correspondence is to be addressed.

Department of Chemistry and Center for Catalysis Research and Innovation

University of Ottawa

10 Marie Curie Private

Ottawa, Ontario, Canada K1N 6N5

Tel.: +1 613 562 5800 ext. 2018; Fax: +1 613 562 5170

E-mail: dbryce@uottawa.ca

Table S1. Experimental parameters used for the acquisition of ^{13}C, ^{31}P, and ^{77}Se NMR CP/MAS spectra.

compound	B_o / T	nuclide	window / kHz	points	MAS / Hz	$\pi/2$ pulse / µs	scans	contact times/ µs	recycle delay / s	decoupling
1	9.4	^{13}C	340	3k	8k	3.25	4204	5000	35	Spinal64
	9.4	^{31}P	400	4k	3k	2.5	307	5000	6	TPPM
	11.75	^{31}P	494	4k	10k	4.5	2865	2000	20	CW
	9.4	^{77}Se	494	4k	6.5k	3.75	5568	20000	30	CW
	9.4	^{77}Se	1489	2k	8k	3.75	2512	20000	34	CW
2	9.4	^{13}C	338	3k	5k	3.25	1200	5000	10	Spinal64
	9.4	^{31}P	400	4k	2.1k	2.5	504	5000	6	TPPM
	11.75	^{31}P	494	4k	10k	4.5	1089	2000	30	CW
	9.4	^{77}Se	1489	4k	3.2k	3.70	6592	20000	20	CW
	9.4	^{77}Se	820	6k	5k	7.0	2392	5000	100	CW
	11.75	^{77}Se	1048	8k	3k	2.8	1024	20000	100	CW
	21.1	^{77}Se	1533	8k	10k	4.0	2560	20000	30	CW
3	9.4	^{13}C	354	3k	10k	3.50	6060	2000	15	Spinal64
	9.4	^{31}P	400	4k	3k	3.00	600	5000	5	TPPM
	11.75	^{31}P	494	4k	10k	4.50	2400	2000	30	CW
	9.4	^{77}Se	494	4k	5.5k	3.75	3280	20000	30	CW
	9.4	^{77}Se	1489	4k	8k	3.75	2744	20000	30	CW

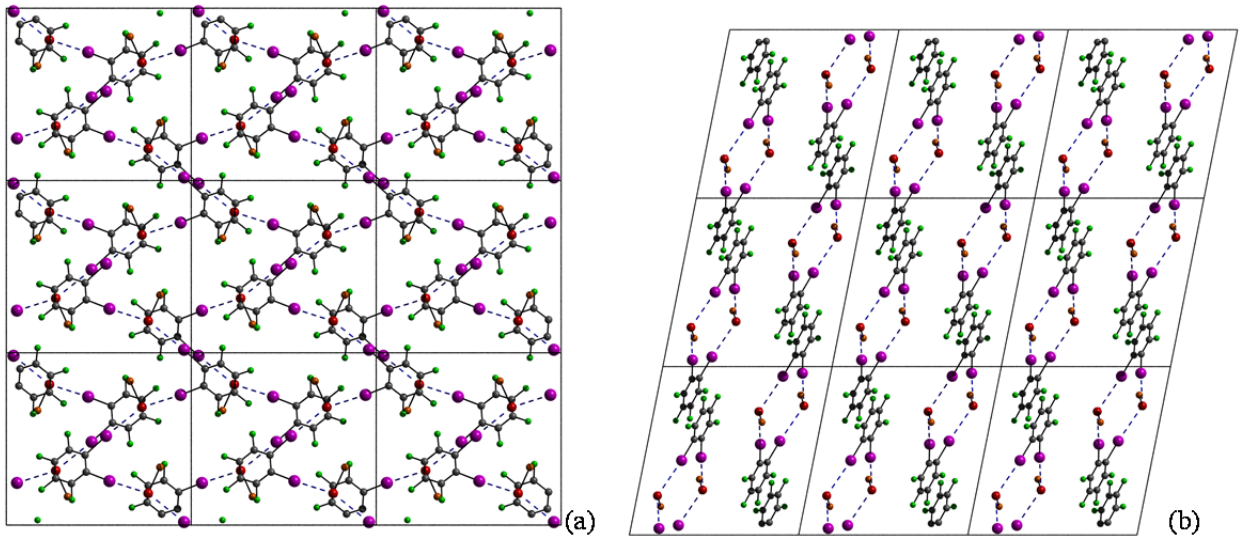

Figure S1. Crystal packing of **2** in a 3 x 3 x 3 unit cell viewed along the *a* axis (a) and *b* axis (b). In (b) the two 1D zigzag chains are observed. The phenyl rings on P are omitted to more clearly show the network.

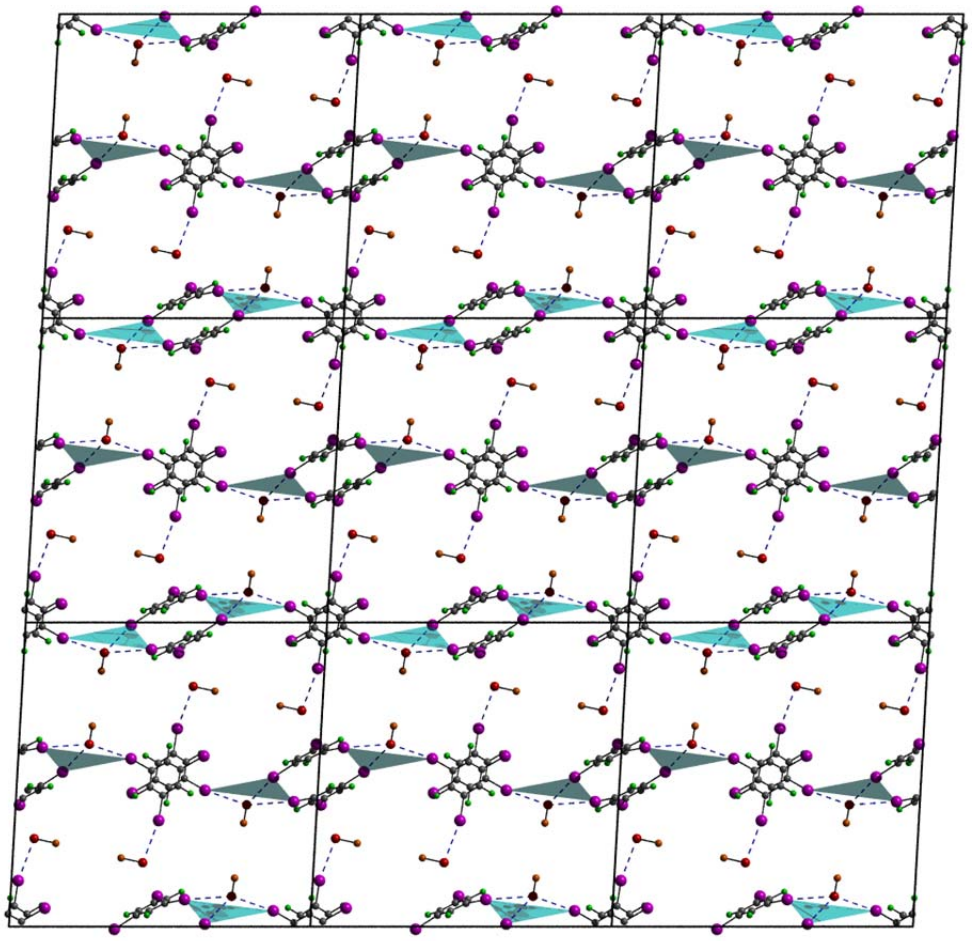

Figure S2. Crystal packing of a 3 x 3 x 3 unit cell for **3** along the *b* axis. There are two crystallographically unique selenium sites in **3**. One is highlighted by the blue surface of a polyhedron which forms a one dimensional zigzag chain along the *b* axis. The second site is within a discrete entity between the zigzag chains. The phenyl rings on P are omitted for clarity.

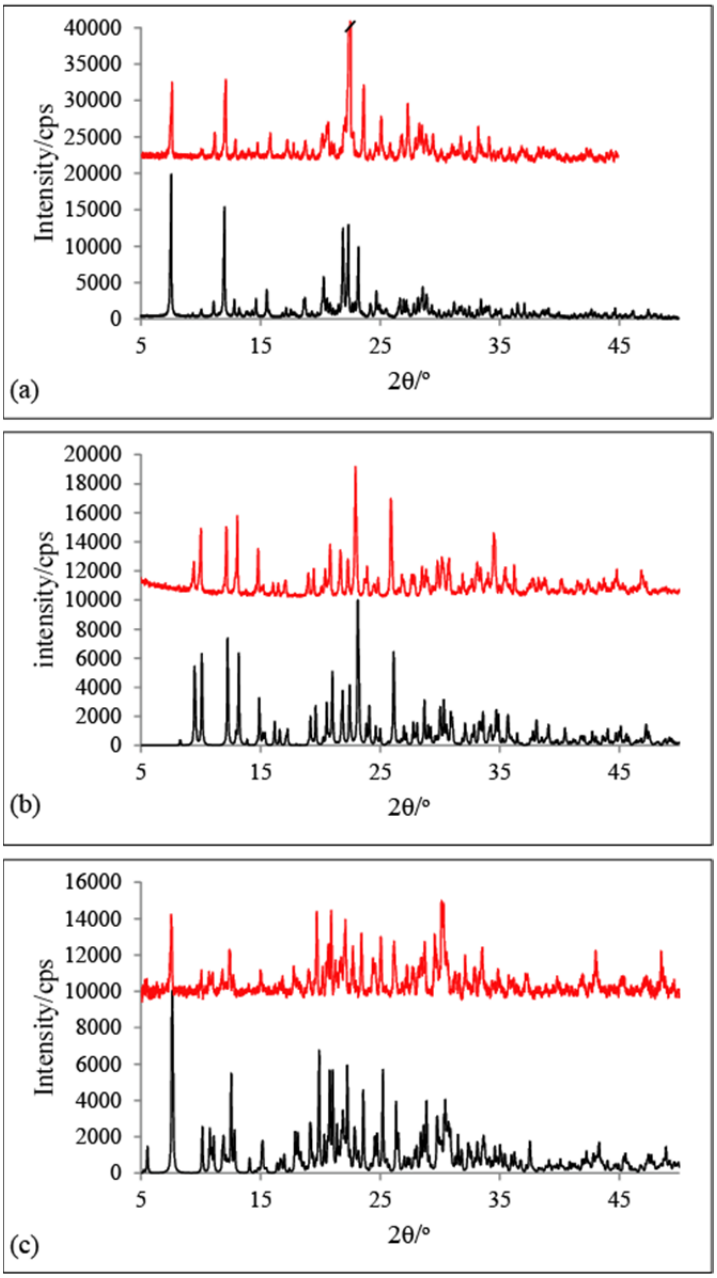

Figure S3. Experimental powder X-ray diffraction patterns (red trace) for (a) (Ph_3PSe)(*p*-DITFB), (b) (Ph_3PSe)(*o*-DITFB), (c) (Ph_3PSe)(*sym*-TITFB) along with simulations in black based on single crystal X-ray data. All experiments were carried out using a Rigaku Ultima IV instrument with 2θ ranging between 5 and 50° in increments of 0.02° at a rate of 0.6° per minute. Simulations were generated using Mercury software available from the Cambridge Crystallographic Data Centre.

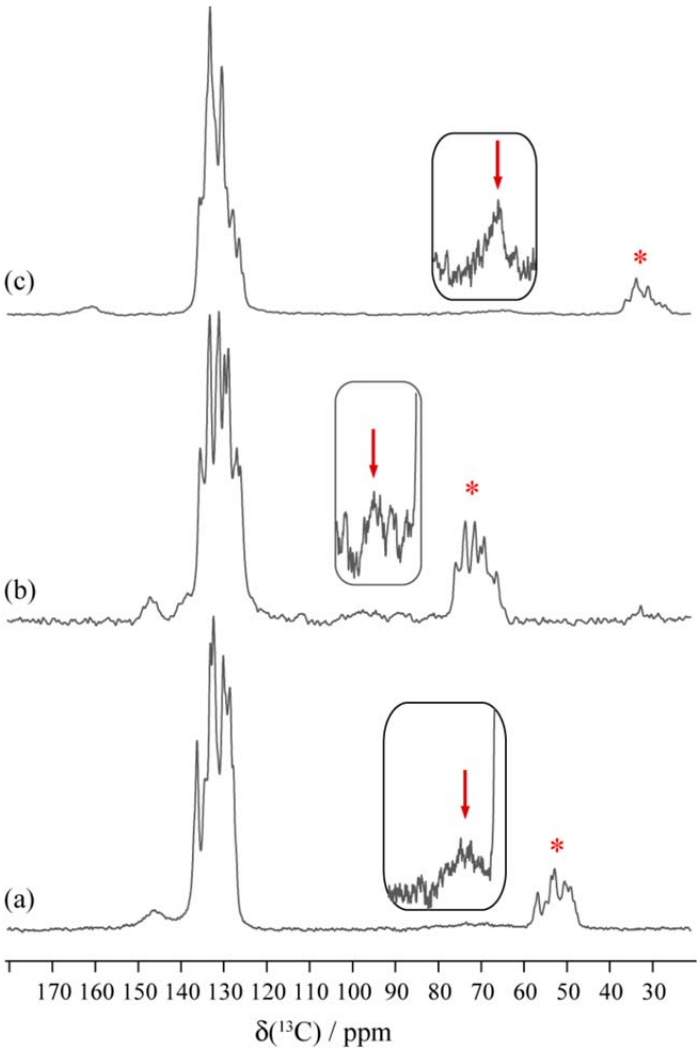

Figure S4. Experimental ^{13}C CP/MAS solid-state NMR spectra acquired at 9.4 T are presented for (a) (Ph_3PSe)(*p*-DITFB) with a MAS rate of 8 kHz, (b) (Ph_3PSe)(*o*-DITFB) with a MAS rate of 5 kHz, and (c) (Ph_3PSe)(*sym*-TITFB) with a MAS rate of 10 kHz. Red asterisks indicate spinning sidebands and the inset shows a vertical expansion of the C-I region. The peaks of interest, particularly in (b), were further identified by experiments at different MAS rates.

(Ph_3PSe)(*p*-DITFB) ^{13}C NMR: 146.0 (b, C-F(DITFB)),136.7-127.9 (m, Ph_3PSe), 73.4 (C-I, DITFB).

(Ph_3PSe)(*o*-DITFB) ^{13}C NMR: 147.0 (b, C-F(DITFB)),135.6-125.9 (m, Ph_3PSe), 97.6 (C-I, DITFB).

(Ph_3PSe)(*sym*-TITFB) ^{13}C NMR: 161.0 (b, C-F(TITFB)),135.4-126.5 (m, Ph_3PSe), 65.3 (C-I, TITFB).

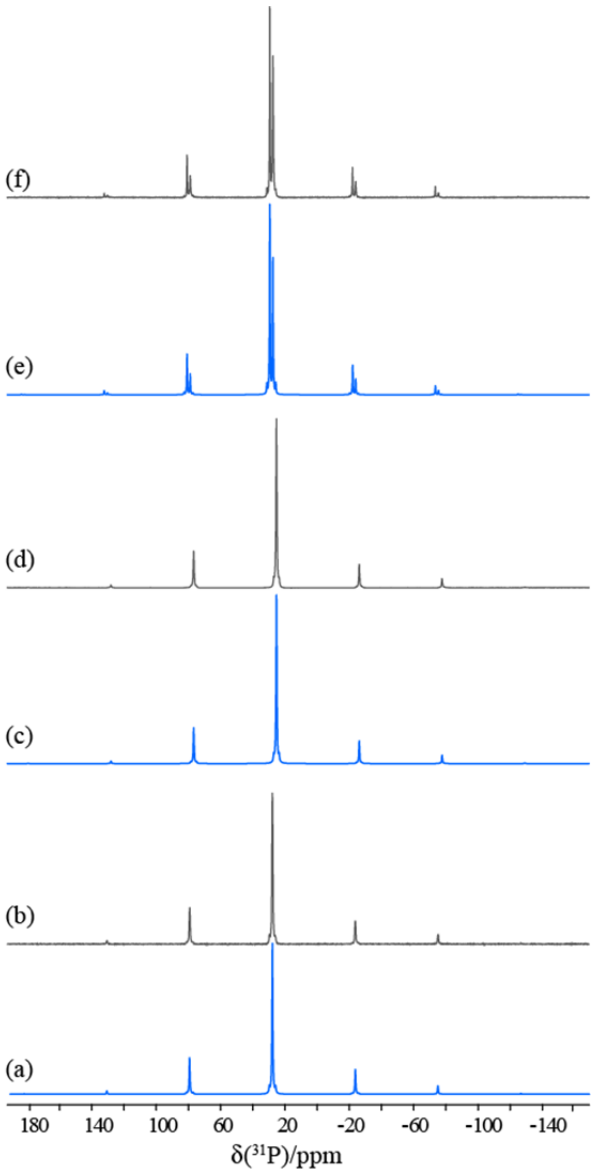

Figure S5. Experimental ^{31}P CP/MAS solid-state NMR spectra acquired at 11.75 T with a spinning frequency of 10 kHz are presented for (b) (Ph_3PSe)(*p*-DITFB), (d) (Ph_3PSe)(*o*-DITFB), (f) (Ph_3PSe)(*sym*-TITFB). Their respective simulated spectra are shown in blue ((a), (c) and (e)).

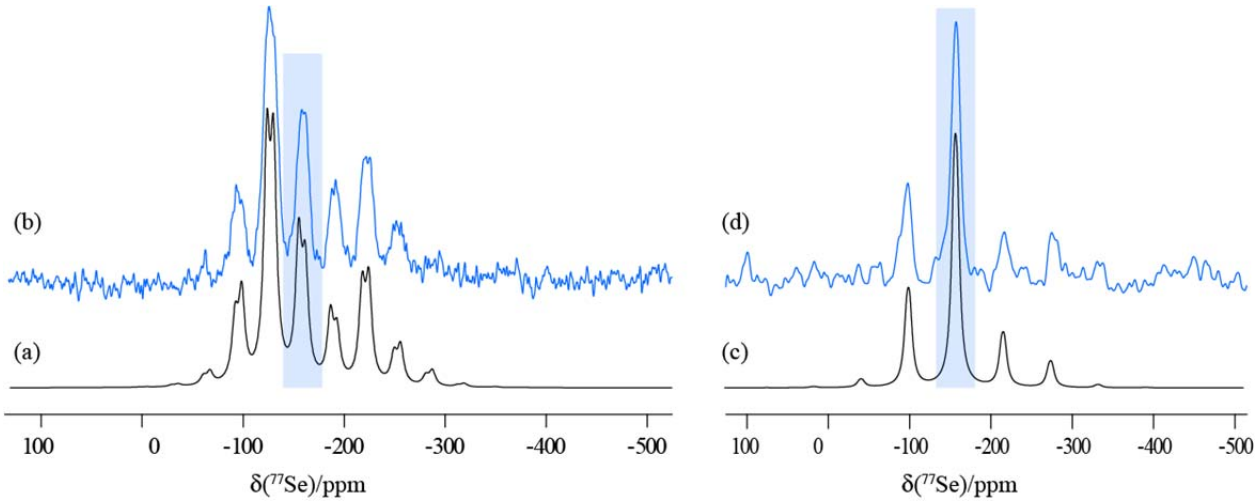

Figure S6. Experimental ^{77}Se CP/MAS solid-state NMR spectra of (Ph_3PSe)(*o*-DITFB) acquired at 11.75 T with a spinning frequency of 3 kHz (b) and at 21.1 T with a spinning frequency of 10 kHz (d). Their respective simulated spectra are in black ((a) and (c)). A long relaxation time constant (T_1) hindered the acquisition of a spectrum with good signal-to-noise at 21.1 T in a reasonable time.

Table S2. Calculated ^{31}P Chemical Shift Tensors.

	compound		method[a]	δ_{iso} / ppm	Ω / ppm	κ
	Ph_3PSe	site 1	ZORA	48.1	203	0.57
		site 1	TPSS	19.7	208	0.68
		site 2	ZORA	43.8	200	0.51
		site 2	TPSS	20.6	207	0.63
1	(Ph_3PSe)(*p*-$C_6F_4I_2$)	site 1	ZORA	51.6	177	0.32
		site 1	TPSS	55.9	189	0.79
		site 2	ZORA	37.3	157	0.79
		site 2	TPSS	60.0	177	0.48
2	(Ph_3PSe)(*o*-$C_6F_4I_2$)	site 1	ZORA	46.5	143	0.82
		site 1	TPSS	57.5	161	0.87
3	(Ph_3PSe)(*sym*-$C_6F_3I_3$)	site 1	ZORA	61.7	179	0.68
		site 1	TPSS	62.3	176	0.71
		site 2	ZORA	57.0	159	0.65
		site 2	TPSS	55.5	149	0.74

a. ZORA indicates a GGA revPBE calculation including scalar relativistic effects carried out in ADF with the ZORATZP basis set. TPSS indicates a calculation carried out with the TPSS functional in Gaussian 09 with the 6-311G** basis set.

Table S3. Calculated ^{77}Se Chemical Shift Tensors and $J(^{77}Se,^{31}P)$ Coupling Constants

	compound		method[a]	δ_{iso} / ppm	Ω / ppm	κ	$J(^{77}Se, ^{31}P)$ / Hz
	Ph_3PSe	site 1	ZORA	29.1	420	0.17	-689
		site 1	TPSS	-19.4	371	0.11	-645
		site 2	ZORA	37.5	436	0.28	-689
		site 2	TPSS	-21.6	383	0.26	-645
1	(Ph_3PSe)(*p*-$C_6F_4I_2$)	site 1	ZORA	27.0	224	-0.19	-678
		site 1	TPSS	93.4	189	0.22	-635
		site 2	ZORA	162.1	428	0.02	-628
		site 2	TPSS	238.0	405	0.06	-587
2	(Ph_3PSe)(*o*-$C_6F_4I_2$)	site 1	ZORA	166.2	365	0.14	-619
		site 1	TPSS	234.0	335	0.09	-579
3	(Ph_3PSe)(*sym*-$C_6F_3I_3$)	site 1	ZORA	108.8	428	0.14	-678
		site 1	TPSS	191.2	409	0.12	-616
		site 2	ZORA	219.9	326	0.85	-616
		site 2	TPSS	272.1	317	0.88	-573

a. ZORA indicates a GGA revPBE calculation including scalar relativistic effects carried out in ADF with the ZORATZP basis set. For chemical shifts, TPSS indicates a calculation carried out with the TPSS functional in Gaussian 09 with the 6-311G** basis set. For *J* couplings, TPSS indicates a calculation carried out in ADF with the TPSS functional and ZORATZP basis set, with scalar relativity.

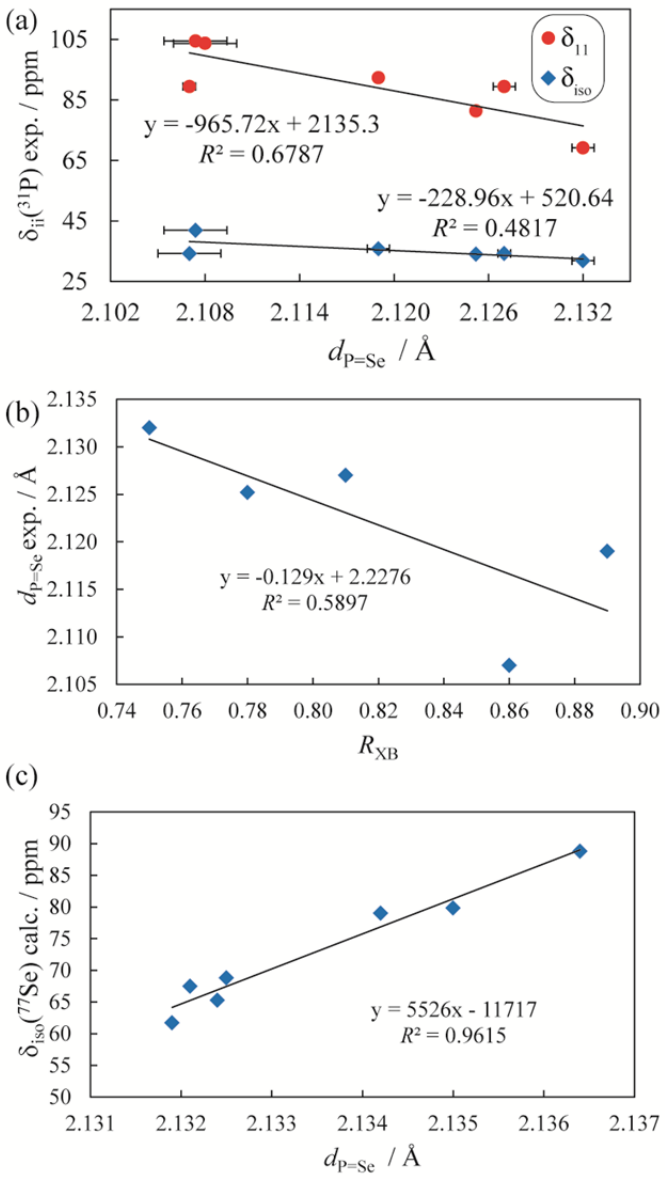

Figure S7. (a) Experimental ^{31}P chemical shifts as a function of the selenium-phosphorus distances, $d_{P=Se}$. (b) Selenium-phosphorus distances as a function of the cumulative halogen bond reduced distance parameter, R_{XB}. (c) ZORA calculated ^{77}Se isotropic chemical shifts as a function of $d_{P=Se}$. For (c), computations (ZORA revPBE) were performed on a cluster model ($(CH_3)_3PSe\cdots ICF_3$) where the I···Se distance was increased by increments of 0.04 Å between 3.40 (R_{XB} = 0.85) and 3.66 Å (R_{XB} = 0.92) and kept fixed while the model was geometry optimized.

Table S4. Hybridization/polarization analysis of NLMOs.[a,b]

compound		NLMO #	Orbital type/%	Percent from parent NBO/%	Atomic hybrid contribution
1 (Ph_3PSe)(*p*-$C_6F_4I_2$)	Site 1	161	LP Se	0.14 I	1s(10.28%)p8.56(87.94%)d0.17(1.78%)
				98.72 Se	27s(87.52%)p0.14(12.47%)d0.00(0.01%)
		61	BD P-Se	0.06 I	1s(9.83%)p9.01(88.51%)d0.17(1.66%)
				46.26 Se	27s(12.61%)p6.86(86.56%)d0.07(0.82%)
				52.14 P	28s(32.63%)p2.05(66.79%)d0.02(0.57%)
	Site 2	238	LP Se	0.11 I	1s(10.43%)p8.43(87.91%)d0.16(1.67%)
				98.74 Se	35s(87.83%)p0.14(12.16%)d0.00(0.01%)
		76	BD P-Se	0.06 I	1s(12.08%)p7.15(86.35%)d0.131.57%)
				46.48 Se	35s(12.19%)p7.13(86.97%)d0.07(0.83%)
				51.78 P	36s(31.32%)p2.17(68.09%)d0.02(0.58%)
2 (Ph_3PSe)(*o*-$C_6F_4I_2$)		238	LP Se	0.14 I	1s(9.37%)p9.51(89.05%)d0.17(1.58%)
				98.66 Se	35s(87.94%)p0.14(12.04%)d0.00(0.01%)
		201	Cr Se	98.98 Se	1s(9.37%)p9.51(89.05%)d0.17(1.58%)
				0.01 P	36s(20.40%)p2.80(57.16%)d1.10(22.45%)
3 (Ph_3PSe)(*sym*-$C_6F_3I_3$)	Site 1	195	LP Se	0.07 I	1s(8.92%)p10.04(89.65%)d0.16(1.43%)
				98.85 Se	31s(87.59%)p0.14(12.40%)d0.00(0.01%)
		61	BD P-Se	0.04 I	1s(6.90%)p13.28(91.65%)d0.21(1.45%)
				46.13 Se	31s(12.51%)p6.93(86.66%)d0.07(0.83%)
				52.17 P	32s(32.16%)p2.09(67.28%)d0.02(0.57%)
	Site 2	186	LP Se	0.09 I	1s(8.64%)p10.27(88.75%)d0.30(2.61%)
				98.72 Se	4s(87.76%)p0.14(12.22%)d0.00(0.01%)
			BD P-Se	0.05 I	1s(11.26%)p7.70(86.65%)d0.19(2.09%)
				46.71 Se	4s(12.36%)p7.02(86.78%)d0.07(0.86%)
				51.56	5s(31.24%)p2.18(68.16%)d0.02(0.60%)

[a] Selected largest NLMO contributions.

[b] See J. Autschbach, *J. Chem. Phys.*, 2007, **127**, 124106 for further information on the output.

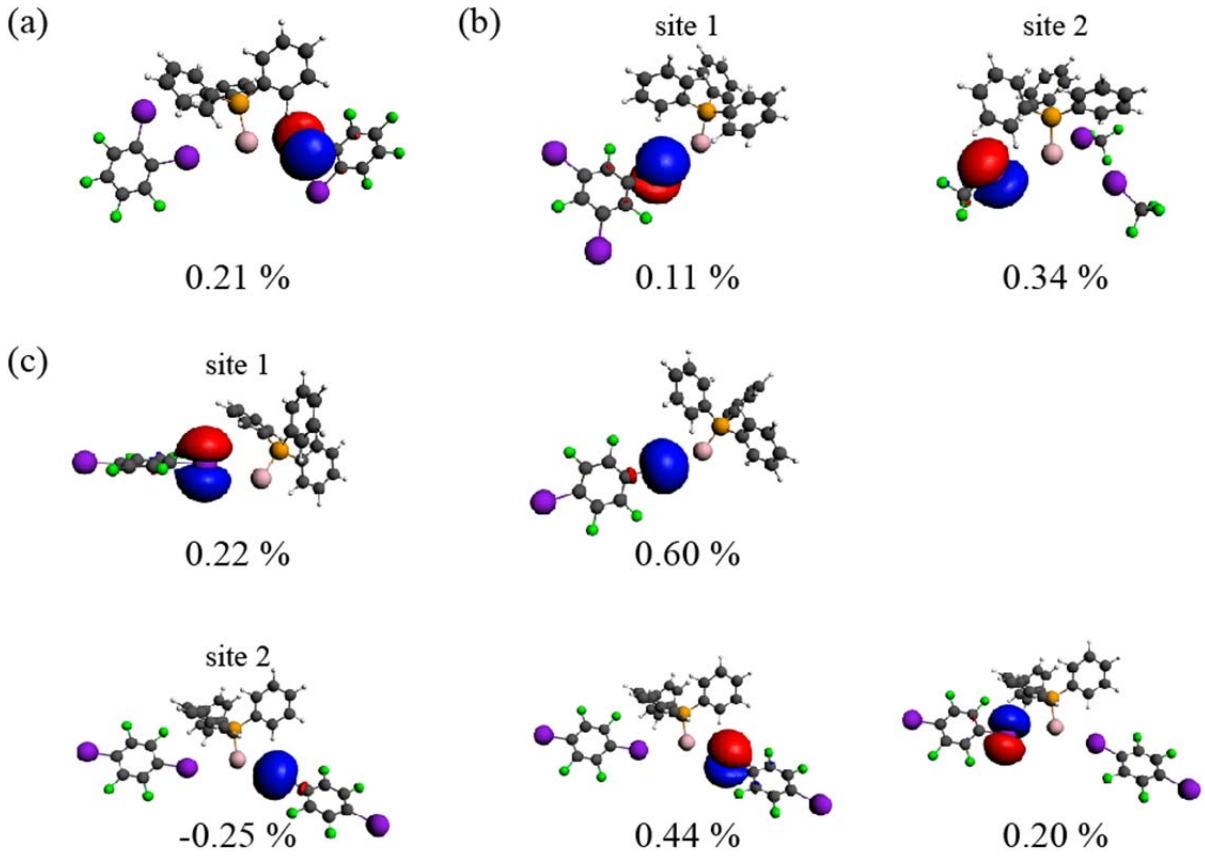

Figure S8. Iodine lone pair NLMOs having the next-largest contributions to the isotropic nuclear spin-spin $J(^{77}Se,^{31}P)$ coupling values in **2** (a), **3** (b), and **1** (c). The percentages underneath the orbitals represent the minor contributions to the $J(^{77}Se,^{31}P)$ coupling values for the XB systems.